23

Design of a compact optical carbon monoxide sensor with a threshold sensitivity of 1 mg/m^3 (0.85 ppm). Evaluation of measurement selectivity

© E.A. Kochelaev, V.V. Petrov

JSC „NPO „Pribor“,
199034 Saint-Petersburg, Russia
e-mail: vladislav-petrov23@mail.ru

Received June 13, 2023
Revised September 19, 2023
Accepted September 20, 2023

The optical scheme of a compact carbon monoxide sensor with a threshold sensitivity level equal to 1 mg/m^3 has been designed. The narrow band filter parameters have been optimized to reduce the sensor's cross-sensitivity to carbon dioxide and water vapor. The optimization takes into account the transmission characteristics of real filters with non-zero transmission in the tail region. For the found filter characteristics, the cross-sensitivity of the sensor was determined to interfering impurities common in cases of fire. Finally, maximum interfering impurity concentration have been evaluated whereby measurement error could be less than the signal from 1 mg/m^3 carbon monoxide.

Keywords: NDIR sensor, optical gas sensor, carbon monoxide, absorption spectroscopy.

DOI: 10.61011/EOS.2023.10.57766.5312-23

Introduction

In many industrialized countries, carbon monoxide poisoning (or CO) is the most widespread type of lethal poisoning [1]. Carbon monoxide is tasteless and odorless and therefore it is especially dangerous for humans. Usually, carbon monoxide enters the atmosphere as result of incomplete combustion of fuel, so operational monitoring of CO is necessary both in production related to combustion processes [2] and in everyday life, for example, in stove-heated houses. The maximum permissible concentration (MPC) of carbon monoxide in air in a working area is 20 mg/m^3 (0.002%) [3].

Along with the issues of safety and environmental monitoring, CO measurement is also important for medical studies, where carbon monoxide is a biomarker of diseases. For a healthy person, a level of CO concentration in exhaled air does not exceed 10 ppm (11.6 mg/m^3) [4, 5]. The listed tasks require application of CO measurement tools with an error up to 1 mg/m^3.

Presently, carbon monoxide is often controlled by using cheap and compact electrochemical sensors. Significant drawbacks of such devices include a limited service life and high cross-sensitivity to hydrogen comparable to the CO response. The latter factor does not allow the use of such instruments at facilities with probable appearance of hydrogen, for example, in shaft mining [2].

The said drawbacks are absent in optical CO sensors. Their design is based on measurement of a transmittance level of the light flux in the infrared (IR) region of the spectrum, which is related to the gas concentration under the Beer–Bouguer–Lambert law. The optical sensors have advantages of high selectivity, durability, potential self-calibration [6]. However, the main obstacle to wider application of the optical instruments is a relatively high cost [6], for example, as compare to the electrochemical sensors.

Table 1 shows the characteristics of the several commercially available optical sensors for carbon monoxide [7–12]. Today, there are a lot of versions of the optical gas analyzers [13], whose cost substantially varies depending on a method of design. Non-dispersive infrared optical sensors (NDIR — non-dispersive infrared) are quite simple in design and have the threshold sensitivity up to 5–10 ppm [7–10]. The opposite end of achievable sensitivity (dozen to hundred ppb) comprises more expensive solutions based on the multi-path optics [14], the laser [15] and correlative [11,12] methods.

In the present study, we have tasked to design an optical scheme for the relatively cheap and compact NDIR CO sensor having the measurement error at most 1 mg/m^3. The level of the measurement error must be kept within the entire operating temperature range, which is accepted to be 0–50°C. We believe that the said measurement error (10% of MPC) is enough for most practical applications. The task was solved by dividing it into several stages. The first stage included determination of an operating spectral range for CO, and selection of an element base of the optical scheme based thereon and design of a sketch of the sensor's optical scheme.

The second stage included selection of parameters of narrow-band IR filters of the sensors that provide maximum selectivity to interfering impurities at the required sensitivity. The selected parameters of the filters were taken to calculate the signal-to-noise ratio for the threshold CO concentration of 1 mg/m^3 based thereon.

Table 1. Characteristics of several commercially available optical CO sensors

Company	Description of item	Method of measurements	Range measurements, ppm	Error, ± ppm
SmartGas [7] (Germany)	F3-222205-05000	NDIR	0–2000	20
	SX-100006-00000		0-1000	6
	SX-200009-00000		0-500	5
Cubic [8] (China)	Gasboard-2050		0-3500	35
Promisense [9] (China)	LARK-1 CO 1000PPM		0-1000	10
	LARK-1LMCT CO 1000PPM		0-1000	2
Euro-Gas [10] (England)	2112B5022-CO		0-2000	20
EcoTech [11] (Australia)	Serinus 30	Cross-flow NDIR	0-200	0.02
Horiba [12] (Japan)	GP-300		0-200	1

The third stage included calculations of the cross-sensitivity to the interfering impurities, which have high probability to appear in fire. The calculations of the second and third stages were done by taking into account characteristics of the real IR filters whose transmittance around the tails does not tend to zero. The calculation has revealed that „non-ideality“ of the filter should have been taken into account, thereby significantly reducing optimistic forecast for the cross-sensitivity of the sensor.

The final calculated threshold sensitivity of the sensor was provided by:

– selection of the strongest CO absorption band;

– design of the optical scheme with a low level of light flux losses;

– application of fast light-emitting diodes and low-noise photodiodes;

– modulation of the light flux at an operating frequency and filtration of noise outside the operating frequency band;

The final selectivity is determined by:

– selection of the position of the central wavelength and the width of the IR filters;

– taking into account non-zero transmittance of the real IR filters around the „tales“.

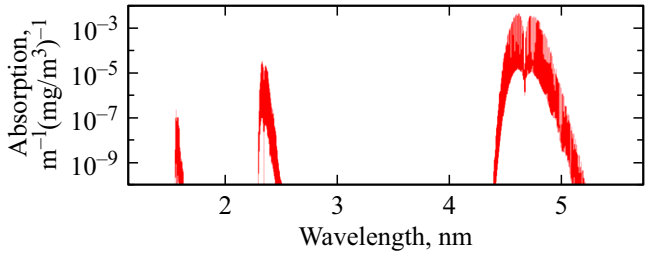

Figure 1. Dependency of the CO absorption coefficient on the wavelength [19].

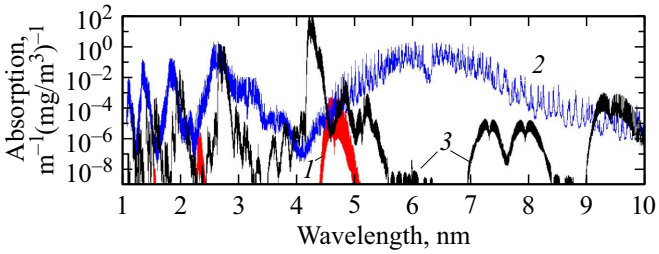

Figure 2. Dependency of the absorption coefficients for CO (*1*), H_2O (*2*) and CO_2 (*3*) on the wavelength [19].

Selection of the operating spectral range

The IR absorption spectrum of carbon monoxide (Fig. 1) consists of a number of bands, whose intensity nonlinearly increases with increase in the wavelength. For the operating range, we have selected the most intensive CO band within 4.6–4.8 μm. The selected spectrum range stays in a window of atmospheric transparency 3–5 μm (Fig. 2) and is often used in measuring carbon monoxide within the IR range [13]. The absorption spectra of such widespread interfering impurities as carbohydrates are neither overlapped with the said CO band.

Optical scheme of the sensor

The designed optical scheme (Fig. 3) of the sensor is based on the widespread version designed with a objective lens being a spherical mirror that is removed from the

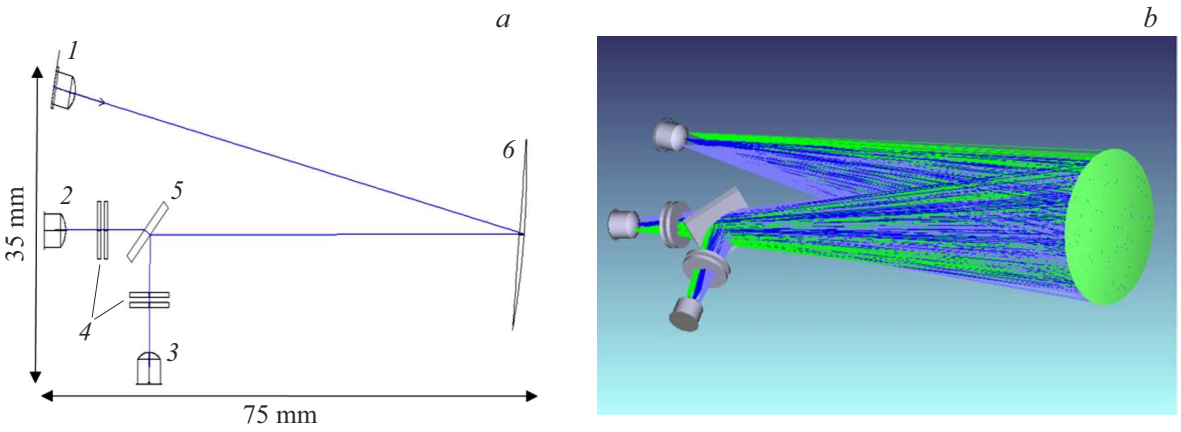

Figure 3. Optical scheme of the CO sensor: *1* — the immersion lens of the light-emitting diode LED 42, *2, 3* — the immersion lenses of the photodiodes PD 47 and PD 42, *4* — the set of the narrow-band filters, *5* — the spectrum-dividing mirror, *6* — the spherical mirror, (*b*) the path of radiation in the optical scheme of the CO sensor.

emitter and the receivers for the double focal distance of 70 mm (radius $R = 70$ mm). The main elements of the scheme also include a light-emitting diode, a gas cuvette with the optical path length 10 cm, a spectrum divider — the interference mirror designed to spectrally divide the two light fluxes, narrow-band interference filters, photodiodes of the measurement and reference channels. Application of the reference photodetector is required for compensation of instability of the light flux that is unrelated to absorption of the gas in the gas cuvette. It can be caused by change of the light power of the emitter, contamination or „aging" of the optics, light scattering on aerosols.

The obtained overall dimensions of the scheme $75 \times 35 \times 30$ mm are resulted from a trade-off between simplicity, compactness, fabricability of the sensor, on one hand, and from a minimum detected signal with appearance of carbon monoxide, on the other hand. It will be shown below that the length of the optical path inside the cuvette 10 cm is enough to ensure the measurement error of the sensor of at most 1 mg/m^3. In case of adjusting the error requirements, the optical scheme can be easily scaled to the required length of the optical path.

The emitter of the CO sensor has been selected to be the light-emitting diode LED 42 produced by „IoffeLED" [16], for which the emitted light power is $30-40\,\mu$W within the spectrum region of $2.8-5.3\,\mu$m. Advantages of the use of the light-emitting diodes over thermal IR sources include compactness, low energy consumption, high performance ($\tau < 10^{-7}$ s). The latter can minimize the noise level in the measurements by: 1) modulability of the light flux of the light-emitting diode at the frequencies up to several MHz, 2) recording of a variable light signal of a specified frequency and filtration of the noise spectrum outside the operating frequency band. The important advantage of the light-emitting diodes is stability of the light power during operation provided that they are thermally stable [6,17]. It favorably distinguishes the light-emitting diodes from the thermal sources prone to aging effects [6]. However, the very necessity of thermal stabilization due to dependency of the spectral power density on the temperature (Fig. 4) increases the cost of the light-emitting diode and the sensor as a whole, which is certainly a drawback.

In the CO sensor under consideration, the light-emitting diode LED 42 is thermally stabilized by the Peltier element at a lower boundary of the operating temperature range of the sensor — 0°C. The power of the light flux for the said temperature is about $1\,\mu$W and is close to the maximum one (Fig. 5).

The radiation receivers have been selected by us to be the photodiodes „Ioffe Led" PD 47 and PD 42 for the measurement and reference channels, respectively. Application of the photodiodes with detectability of $D^* = 10^{10}-10^{11}$ (W·cm^{-1}·Hz$^{-1/2}$) provides the value of the threshold sensitivity by $1-2$ orders above the sensitivity of the sensors with pyroelectric receivers. It was convenient for us to select the photodiodes produced by the same company for the emitters due to similarity of the optical characteristics of the immersion lenses, the sizes of the emitting and receiving sites (mesas) of the light-emitting diode and the photodiode, respectively. It could minimize the vignetting losses in the scheme when transferring the image of the emitting mesa to the surface of the photodetection mesa with a single magnification. In order to reduce the threshold sensitivity of the designed sensor, the photodiodes should be thermally stabilized within the low temperatures. When the photo-sensitive site is cooled, its resistance increases and the value of the thermal noise of the photodetector reduces.

The preliminary experimental studies have shown that the temperature radiator selected by us could create a maximum temperature drop between the photodiode mesa and the environment ~ 80°C.Therefore, for stable operation of the sensor at the ambient temperatures up to 50°C, the operating temperature of the photodetector has been selected to be minus 30°C.In accordance with the supplier data, the said temperature is matched to the value of

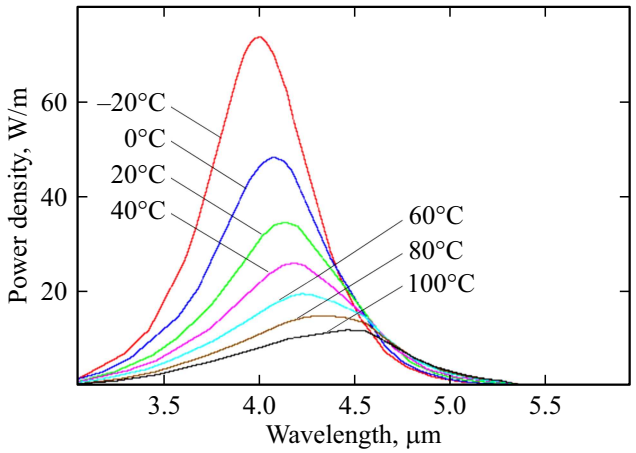

Figure 4. Dependency of the power density of the light diode LED 42 on the wavelength at various temperatures of the light-emitting diode.

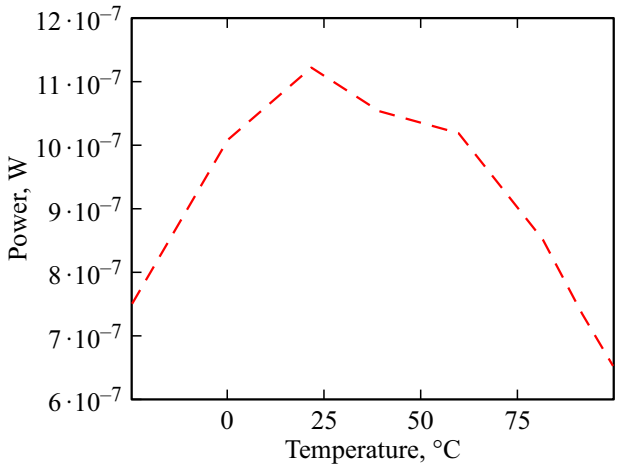

Figure 5. Dependency of the light flux power of the light-emitting diode LED 42, limited by the Gaussian IR filter of 4.6 μm, $\delta = 80$ nm (FWHM), on the temperature of thermal stabilization.

resistance of 300 Ω, which has been then used for noise calculations.

The total transmittance losses $\tau(\lambda)$ in the system are defined by vignetting of the optical scheme elements $\tau_v(\lambda)$, the mirror reflection $\tau_m(\lambda)$, the transmittance losses in the narrow-band filter $\tau_f(\lambda)$, the spectrum-dividing mirror $\tau_s(\lambda)$ and in the cuvette windows $\tau_w(\lambda)$ (No window is depicted on Fig. 3 *a*). Preliminarily, the parameters of the interference spectrum divider can accepted to be ideal $\tau_s(\lambda) \approx 1$. For the cuvette windows, it is proposed to use an antireflection coating $\tau_w(\lambda) \approx 1$. Accordingly, it may be assumed as a first approximation that the total losses are defined by vignetting and reflection (for which transmittance weakly depends on the wavelength) and by transmittance of the wide-band filter as well: $\tau(\lambda) = \tau_v \tau_m \tau_f(\lambda)$. Based on the scheme optimization, by inconsistent analysis in the Zemax-EE software [18] has provided the value of $\tau_v = 0.87$, thereby indicating weak vignetting in the scheme. For the

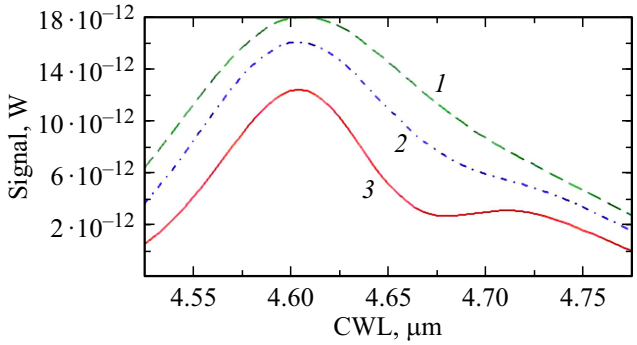

Figure 6. Dependency of the CO signal (1 mg/m^3) on the central wavelength of the IR filter (Gaussian profile). Width of the transmittance band of the filters δ (FWHM) — 150 (*1*), 120 (*2*), 80 nm (*3*).

mirror aluminum coating, it can be assumed in the IR region that $\tau_m = 0.9$. Therefore $\tau(\lambda) \sim 0.78 \cdot \tau_f(\lambda) = \tau_o \cdot \tau_f(\lambda)$, where τ_o — transmittance of the scheme without taking into account transmittance of the narrow-band filter. The full set of data for the emitter and the photodiodes was kindly provided by the supplier — the „IoffeLed“ company.

Determination of the filter parameters

For the designed CO sensor, the measurement error can occur due to a low value of a useful signal, a high level of the instrument noses or due to false positive actuations in the presence of the interfering impurities. Our task was to determine parameters of the narrow-band filter — the width at half maximum δ(FWHM) and the location of the central wavelength λ_c(CWL), for which a signal for the target substance is close to the maximum one, while a signal for the interfering impurities is the lowest possible. H_2O and CO_2, which define absorption of the „clean“ atmosphere within the middle IR region of the spectrum, have been selected as the interfering impurities (Fig. 2). The following concentrations of the substances were used in the calculations: CO — 1 mg/m^3, CO_2 — 3% (54870 mg/m^3), H_2O — 20 g/m^3, which corresponds to 100% humidity at 25°C. For the found characteristics of the IR filter, it has determined: the signal-to-noise ratio and the cross-sensitivity of the sensor to the several widespread interfering impurities.

Taking into account the Beer–Bouguer-Lambert law, when an arbitrary gas appears in the atmosphere, with the concentration N [mg/m^3], the change of the light signal power can be calculated by the formula:

$$P(\lambda_c, \delta) = \int_{\lambda_1}^{\lambda_2} (1 - e^{-k(\lambda)Nd}) P_{LED}(\lambda) G(\lambda_c, \delta, \lambda) \tau_o d\lambda, \quad (1)$$

where $P_{LED}(\lambda)$ — the spectral power density of the light-emitting diode LED 42, $\lambda_1 = 2.8\,\mu$m and $\lambda_2 = 5.3\,\mu$m —

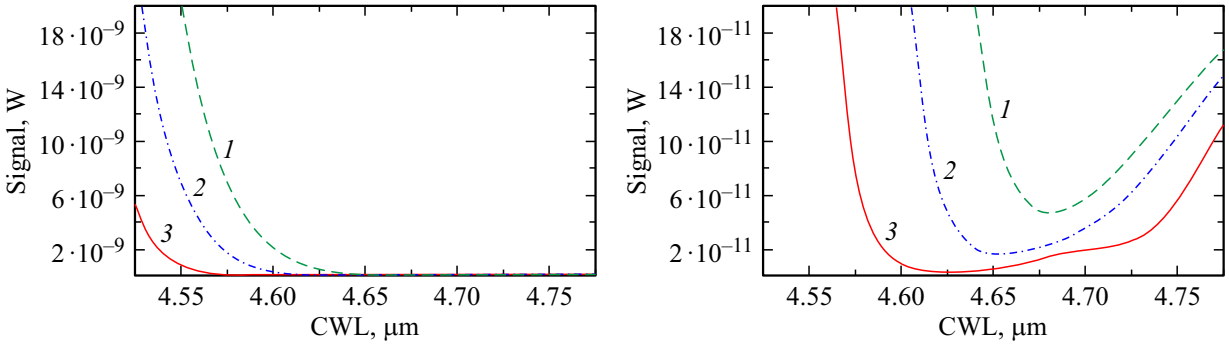

Figure 7. Dependency of the signal of CO_2 (3%) on the central wavelength of the IR filter (Gaussian profile). Filter width δ (FWHM) *1* — $\delta = 150$ nm, *2* — $\delta = 120$ nm, *3* — $\delta = 80$ nm.

the integration limits coinciding with the spectral boundaries of the light-emitting diode radiation, $G(\lambda_c, \delta, \lambda)$ — transmittance of the„ideal" Gaussian filter, for which the width at half maximum is δ(FWHM) and the transmittance maximum at the central wavelength λ_c is 0.8; $\kappa(\lambda)$ — the absorption spectrum of a gas concentration unit in dimensionality $m^{-1}(mg/m^3)^{-1}$ (the data of [19] are used), $d = 0.1$ m — the length of the gas cuvette, $\tau_o = 0.78$ — transmittance of the scheme without taking into account transmittance of the narrow-band filter.

The useful signal of CO $N = 1$ mg/m^3 has been calculated as per (1) to show that the response maximum corresponds to $\lambda_c \sim 4.6\,\mu$m and is $1.2 \cdot 10^{-11}$ W for $\delta = 80$ nm (Fig. 6). The increase in the width δ (FWHM) from 80 to 120 and 150 nm at the fixed λ_c provides an almost proportional contribution to the signal increase. Let us note that the position of the filter of $\lambda_c = 4.6\,\mu$m approximately coincides with the center of the *R*-branch of CO absorption (Fig. 1) is mentioned in the literature when specifying the central wavelength in devices for measurement of carbon monoxide [13].

As the spectrum of CO_2 absorption (Fig. 2) is partially overlapped with edges of the *R*-branch of CO (the center $\sim 4.6\,\mu$m) and substantially overlapped with the *P*-branch of CO (the center $\sim 4.75\,\mu$m), then the value of the CO_2 signal non-linearly increases with the increase in the filter width δ (Fig. 7). In order to minimize the influence of CO_2 on the useful CO signal, we have limited the filter width at the level of $\delta \sim 80$ nm. Technologically, it is more difficult to provide a smaller width without substantial transmittance loss in the maximum λ_c or appreciation of the filter.

When calculating the cross-sensitivity of the interfering impurities, it was reasonable to replace the Gaussian function $G(\lambda_c, \delta, \lambda)$ by the experimental curve of the real filter in (1). Usually, for produced interference filters, transmittance with a distance from the „operating" region of the spectrum increasing, does not tend to zero and can approach several percent. For a sample of the transmittance curve of the real filter, we have used the data for the IR filter produced by „Alcor Technologies" (Saint-Petersburg) with the following characteristics: $\lambda_c \sim 4.574\,\mu$m, $\delta \sim 85$ nm,

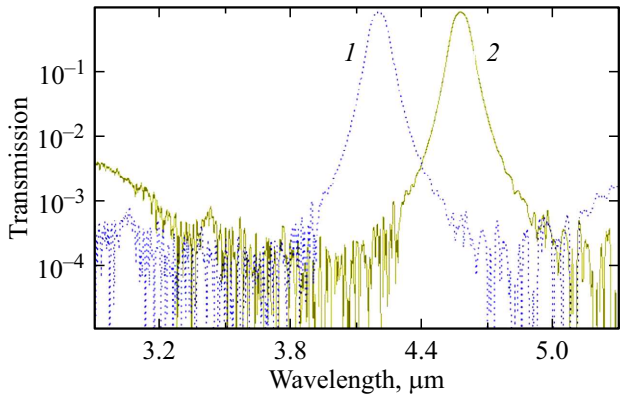

Figure 8. Transmittance of the narrow-band IR light filter produced by „Alcor Technologies" — $\lambda_c \sim 4.2$ (*1*)μm, *2* — $\lambda_c \approx 4.574\,\mu$m.

transmittance around the „tails" $\tau \sim 1\%$ (Fig. 8), transmittance in the maximum of the filter $\tau \sim 0.8$. The said replacement results in transformation of the expression (1) into the expressions:

$$P(\lambda_c) = \int_{\lambda_1}^{\lambda_2} (1 - e^{-k(\lambda)Nd}) P_{LED}(\lambda) R(\lambda_c, \lambda) \tau_o d\lambda, \qquad (2)$$

$$P(\lambda_c) = \int_{\lambda_1}^{\lambda_2} (1 - e^{-k(\lambda)Nd}) P_{LED}(\lambda) R(\lambda_c, \lambda)^2 \tau_o d\lambda, \qquad (3)$$

where $R(\lambda_c, \lambda)$ — transmittance of the real narrow-band filter produced by „Alcor Technologies", whose transmittance center is shifted to the value λ_c (Fig. 8). The expression (2) takes into account installation of one IR filters, so does the expression (3) — that of two. Let us note that the width of the transmittance spectrum of the filter produced by „Alcor Technologies" is close to the calculated value $\delta \sim 80$ nm.

The calculation as per (2) has shown that installation of one IR filter only results in high cross-sensitivity of the measurements to CO_2 (Fig. 9). The obtained result indicates that it is necessary to take into account the characteristics

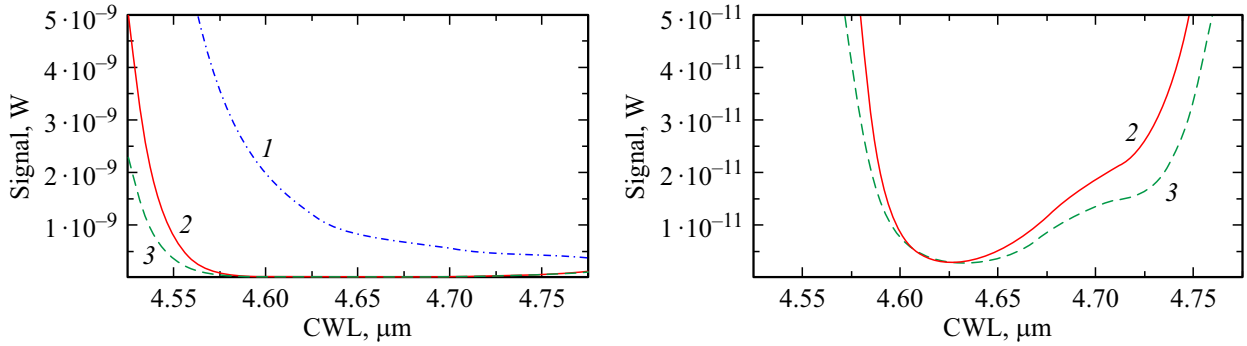

Figure 9. Dependency of the signal of CO_2 3% on the central wavelength of the IR filter. In use: — one (*1*) or two (*2*) filters of „Alcor Technologies“ (λ_c is the same), *3* — the Gaussian filter $\delta = 80$ nm (FWHM).

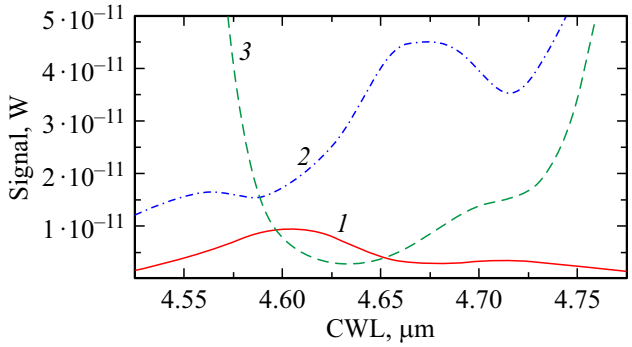

Figure 10. Dependency of the signals on the central wavelength of the IR filter produced by „Alcor Technologies“ (two filters in use): *1* — CO (1 mg/m^3), *2* — H_2O (20 g/m^3), *3* — CO_2 (3%).

of transmittance of the real filter when calculating the selectivity. Therefore, selectivity improvement required either „installation“ of two filters into the model, or manufacturing of the filter with transmittance around the tails $\sim 0.01\%$. In practice, it is cheaper and simpler to implement the first condition. Taking into account the latter, the substance signals were subsequently calculated with two real filters as per the expression (3).

The signals of the sensor (calculated as per (3)) for CO $N = 1$ mg/m^3, CO_2 $N = 3\%$ and water $N = 20000$ mg/m^3 ($N = 20$ g/m^3) are shown on Fig. 10, while Fig. 11 shows selectivity of the CO sensor to the influence of CO2 and moisture. In our calculations, the selectivity β was accepted by us to be a ratio of the value of the signal from 1 mg/m^3 CO to the signal of a respective concentration of the interfering impurity. The reciprocal value of the selectivity is a measurement error expressed in units of CO concentration (for example, with selectivity 2, the error is 0.5 mg/m^3 CO). Also, in order to evaluate the drop in the level of CO sensitivity, the relative level of the CO signal depending on λ_c has been superimposed on the selectivity graph of Fig. 11.

It follows from the shown graphs that for CO_2 and water the most favorable regions of the smaller sensitivity turn out to be spaced apart along the spectrum. The selectivity maximum for CO $_2$ corresponds to $\lambda_c = 4.62\,\mu$m, whereas for water — $\lambda_c = 4.58\,\mu$m. Taking into account that the level of the moisture signal 20 g/m^3 is above the level of the CO signal within the entire range of the wavelengths, then in case of measurement adjustment under the conditions of moisture change by more than 8 g/m^3 ($\beta = 1$, $\lambda_c \approx 4.6\,\mu$m), the instrument design shall reasonably include a cheap moisture sensor with the accuracy readings of $\sim 0.5-1$ g/m^3. In this case, the optimum point λ_c should b selected by referring to the maximum selectivity to CO_2 with allowable drop in the sensitivity to CO. For our sensor, we have selected the central wavelength of the IR filter $\lambda_c = 4.61\,\mu$m, for which the selectivity $\beta = CO_{N=1\ mg/m^3}/CO_{2\,N=3\%}$ is close to the maximum one and is equal to $\beta = 2.4$. The level of sensitivity to CO for $\lambda_c = 4.61$ drops only by 5% and is also close to the maximum one. The selectivity to water $\lambda_c = 4.61$ is 0.4, and it is approximately by 33% less than the maximum value (for $\lambda_c = 4.58$ the selectivity to water $N = 20$ g/m^3 is about 0.6). If the design has no moisture sensor, then the moisture changes by more than ± 8 g/m^3 should be excluded in the operating conditions. For CO_2, at $\beta = 1$ and $\lambda_c = 4.61\,\mu$m, the maximum allowable concentration not causing the errors above 1 mg/m^3 for CO, is $N = 7.2\%$ ($7.2\% = 3\% \cdot 2.4$).

Determination of the signal-to-noise ratio

The found values of λ_c and δ made it possible to determine the level of the signal-to-noise ratio. The power of the useful signal, as calculate as per (3) for $\lambda_c = 4.61\,\mu$m, is equal to $8.8 \cdot 10^{-12}$ W. The average value of the signal at the receiver is determined by the expression:

$$P_0 = \int_{\lambda_1}^{\lambda_2} P_{LED}(\lambda) R(\lambda_c, \lambda)^2 \tau_o d\lambda \approx 3.8 \cdot 10^{-7}\ \text{W}.$$

Therefore, a portion of the power of the useful signal from its average value is about $2 \cdot 10^{-5}$.

When evaluating the noise level, we have taken into account the current I_{oa} and volt U_{oa} noise of an operational

amplifier (OA), the shot noise I_{shot}, as well as the thermal noise of the photodetector I_{heat}:

$$I_n(R) = 2\sqrt{\left(I_{oa}^2 + \left(\frac{U_{oa}}{R}\right)^2 + I_{\text{shot}}^2 + I_{\text{heat}}^2\right)\Delta f}$$

$$= 2\sqrt{\left(I_{oa}^2 + \left(\frac{U_{oa}}{R}\right)^2 + 2eI_o + \frac{4kT}{R}\right)\Delta f}, \qquad (4)$$

where $I_{\text{shot}} = \sqrt{2eI_0}$ [20], e — the electron charge, I_0 — the average value of current through the photodiode (for the photodiode, the current sensitivity is close to 1 A/W, therefore, $I_0 = 3.8 \cdot 10^{-7}$ A), $I_{\text{heat}} = \sqrt{\frac{4KT}{R}}$, $K = 1.38 \cdot 10^{-23}$ J/K — the Boltzmann constant, $T = 303$ K — the photodiode temperature, R — the photodiode resistance, Δf — the width of the frequency band of the electric path as defined by the level of decay of 3 dB, $\Delta f = 1/(2\pi\tau)$ [20], τ — the time constant of the electric path.

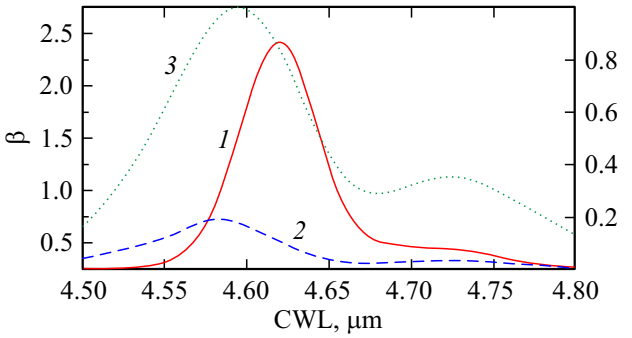

Figure 11. Dependency of the selectivity β on the central wavelength of the IR filter produced by „Alcor Technologies“: *1* — $\beta = CO_{N=1\text{ mg/m}^3}/CO_{2\,N=3\%}$, *2* — $\beta = CO_{N=1\text{ mg/m}^3}/H_2O_{N=20\text{ g/m}^3}$, *3* — the signal of CO 1 mg/m^3 from the central wavelength, which is normalized to the maximum value.

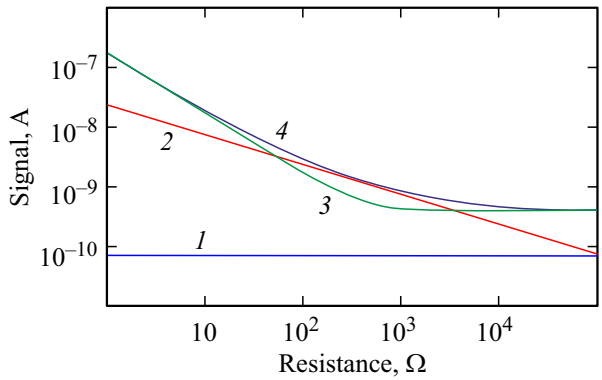

Figure 12. Dependency of the noise value on the resistance of the photodiode mesa. *1* — the contribution of the shot noise; *2* — the contribution of the thermal noise of the photodiode PD 47; *3* — the contribution of the OA noise; *4* — here, it takes into account the total contribution of all the listed sources of noise.

For the designed sensor, we have accepted that $\tau = 1$ s, $\Delta f = 0.16$ Hz, for the OA of the first cascade for amplification of the electric path, the low-noise amplifier AD797 with the value $I_{oa} = 2 \cdot 10^{-12}\,\text{A(Hz)}^{-1/2}$, $U_{oa} = 0.9 \cdot 10^{-9}\,\text{V(Hz)}^{-1/2}$ has been selected. The number 2 before the square root of the expression (4) means that the noise was evaluated in accordance with the level ±2RMS (95% probability for the normal law for error distribution).

Fig. 12 shows the results of calculation as per (4) for the dependency of the noise level $I_n(R)$ on the resistance of the photodiode mesa. Fig. 12 also shows the graphs $I_n(R)$ provided that the noise was defined by the contribution of the individual components: only by the operational amplifier, the shot noise or by the thermal noise of the photodetector PD 47. It follows from the graphs that within the resistance region of 100–3000 Ω the main noise source is the thermal noise of the photodetector, so outside the said area is the noise of the operational amplifier. For the selected temperature of the photodiode −30°C, the resistance is about 300 Ω and as per (4) the noise current is $I_n = 6.4 \cdot 10^{-12}$ A. Accordingly, the signal-to-noise ratio is $I(1\text{ mg/m}^3\text{ CO})/I_n = 8.8 \cdot 10^{-12}\text{ A}/6.4 \cdot 10^{-12}\text{ A} \approx 1.4$.

Selection of characteristics of the reference channel's filter

For the designed CO sensor, it was planned to improve the long-term stability of the measurements by introducing a reference channel being insensitive to the target gas [17] into the system. In this case, the change of the light flux unrelated to gas appearance (for example, as a result of change of the emitter power, contamination or „aging“ of the optics, scattering of radiation on aerosols) should cause similar relative changes of the signals in the measurement and reference channels. Normalizing the measurement channel to the signal of the reference channel can substantially reduce the sensitivity of the measurements to the said external factors and to ensure self-calibration of the sensor and, as a consequence, the high long-term stability.

When selecting the characteristics of the IR filter of the reference channel λ_c, δ , two conditions were to be met:

— the reference channel's sensitivity to CO should be by 1–2 orders below the measurement channel's response to CO;

— the sensitivity to CO_2 $N = 3\%$ and water $N = 20$ g/m^3 should not exceed the level of response to 1 mg/m^3 CO (the level of the signal should be below $8.8 \cdot 10^{-12}$ W).

Similar to the calculation of the measurement channel's filters, using one real filter and increase in the width of the transmittance band width of the filter δ results in non-linear increase in the sensitivity to CO_2 and water. In this regard, for the reference channel, we have also limited the width by the level $\delta \approx 80$–90 nm and introduce a requirement for installation of two filters.

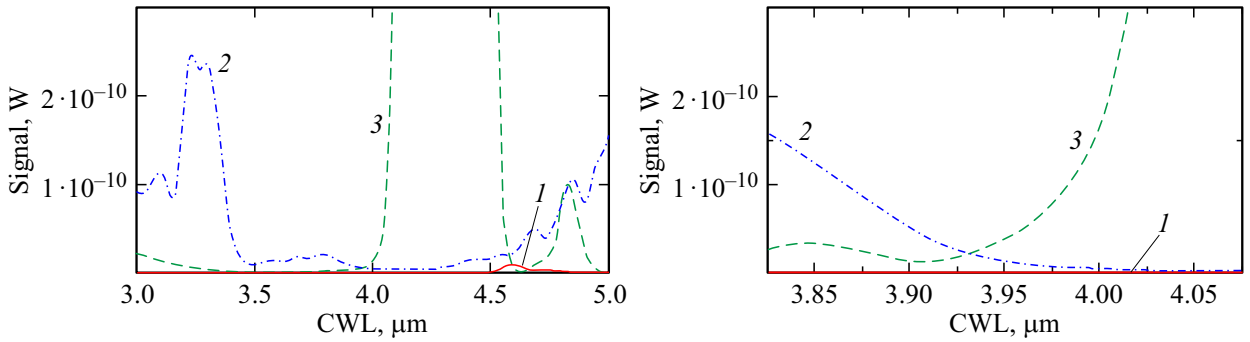

Figure 13. Dependencies of the reference channel's signals on the central wavelength of the IR filter produced by „Alcor Technologies", as measured when using the two filters (*a*) and their portions in the vicinity of 3.95 μm (*b*): *1* — CO (1 mg/m^3), *2* — H_2O (20 g/m^3), *3* — CO_2 (3%).

Table 2. Calculated values of selectivity and limit concentrations of the impurities

Interfering impurity	Impurity concentration, N_p mg/m^3	Selectivity β_{tlv}		Maximum concentration C_{lim}, mg/m^3 ($\beta = 1$)	
		$\lambda_c = 4.61\,\mu$m	$\lambda_c = 3.92\,\mu$m	$\lambda_c = 4.61\,\mu$m	$\lambda_c = 3.92\,\mu$m
H_2O	20000	0.4	3.3	8000	66000
CO_2	3%	2.4	4.9	7.2%	14.7%
NO	0.5	$3.0 \cdot 10^9$	$1.8 \cdot 10^7$	100%	100%
NO_2	0.5	$2.0 \cdot 10^7$	$2.2 \cdot 10^8$	100%	100%
N_2O	0.5	3.7	5.4	1.85	2.7
H_2S	1	$7.6 \cdot 10^5$	$1 \cdot 10^3$	$7.6 \cdot 10^5$	$1 \cdot 10^3$
CH_4	50	788	1.9	$3.9 \cdot 10^4$	95.0
C_2H_6	50	$6.0 \cdot 10^4$	$6.0 \cdot 10^4$	$3.0 \cdot 10^6$	$6.0 \cdot 10^6$
HCl	0.5	$1.6 \cdot 10^5$	$1.2 \cdot 10^4$	$8.0 \cdot 10^4$	$6.0 \cdot 10^3$
HBr	1	$3.3 \cdot 10^7$	60	$3.3 \cdot 10^9$	60
HF	0.05	$2.4 \cdot 10^{11}$	$2.9 \cdot 10^9$	100%	100%
NH_3	0.8	$5.3 \cdot 10^4$	288.8	$4.2 \cdot 10^4$	231
H_2CO	0.8	$7.5 \cdot 10^6$	$3.3 \cdot 10^4$	$6.0 \cdot 10^6$	$2.6 \cdot 10^4$
SO_2	0.5	$3.9 \cdot 10^8$	229.1	100%	114.6
HCN	1	$3.7 \cdot 10^3$	370.0	$3.7 \cdot 10^3$	370
$C_2H_5OH^*$	10	4	7.6	40	76

*Note.** Data based on the WebBook base [21] (spectrum resolution of 0.1 cm^{-1}).

The calculation done by the formula (3) has shown that the radiation range of the light-emitting diode LED 42 $\lambda = 2.8-5.3\,\mu$m comprised no CO response for all the wavelengths except for the region near 4.6 μm (Fig. 13, *a, b*). Taking into account a form of the CO absorption spectrum (Fig. 2), these results were expected.

Comparing the signals of CO_2 $N = 3\%$ and water $N = 20$ g/m^3, it can be noted that only around 3.9 μm their level does not exceed the value of the response of the useful signal of CO 1 mg/m^3 ($\sim 10^{-11}$ W). For the reference channel's filter, we have selected the central wavelength $\lambda_c = 3.92\,\mu$m — this point is located near intersection of the signal graphs and corresponds to almost minimum sensitivity to CO_2 and the relatively low sensitivity to water. Let us note that usually the literature specifies the region around 3.9 μm as a reference channel, but at the same time it has no details about allowable spread of the filter characteristics.

Based on the results obtained, these data can be calculated. For example, when limiting the allowable error of the reference channel readings by ± 0.5 mg/m^3 CO, the allowable spread of the central wavelength of the filter $\lambda_c = 3.92 \pm 0.03\,\mu$m.

Calculation of the selectivity of the measurement and reference channels of the CO sensor

The cross-sensitivity of the sensor was calculated based on the spectrum database Hitran [19] (Table 2). The list of the interfering impurities included the substances which can appear in fire together with CO. Table 2 additionally

included methane, ethane and ethanol, the experimental spectrum of the latter is available in the database NIST Chemistry WebBook [21]. The signals of the individual gases were calculated based on the expression (3), which had used the found values of the central wavelengths of the IR filters $\lambda_c = 4.61\,\mu$m and $\lambda_c = 3.92\,\mu$m, respectively, for the measurement and reference channels. As before, the selectivity (β_{tlv}) was calculated as a ratio of the signal of CO $N = 1\,\text{mg/m}^3$ to the signal of the corresponding concentration of the impurity as specified in the table. Initially, the calculation was done by taking the substance concentrations N_p, which are either close or equal to the MPC level. Then, based on the obtained data, the formula

$$C_{\text{lim}} = N_p \cdot \beta_{tlv}$$

was used to calculate the impurity limit concentration C_{lim}, in whose presence the error does not exceed $1\,\text{mg/m}^3$ by the level of CO (the signal below $8.8 \cdot 10^{-12}\,\text{W}$).

As follows from Table 2, for most of the substances, the selectivity turns out to be quite high. The smaller value of the selectivity turns out to be for CO_2, nitrous oxide N_2O, methane, ethanol $2 < \beta_{tlv} < 4$. As mentioned above, for $20\,\text{g/m}^3$ water, $\beta_{tlv} = 0.4$. Thus, the calculation shows that due to diversity of the spectra of the interfering impurities for the two spectrum ranges, it is difficult to ensure a high selectivity simultaneously for all the substances. Such interfering impurities as methane, hydrogen bromide, hydrogen cyanide exhibit the high selectivity only for the measurement channel and the significantly smaller selectivity for the reference channel.

Based on the obtained data, it is possible to evaluate limits of applicability of the designed sensor. The limit concentrations of the interfering impurities, at which $\beta = 1$, are shown in Table 2 in the last two columns. If the said cross-sensitivity is not enough for specific application, then the sensor sensitivity can be increased by:

— adjustment of the readings obtained via a parallel measurement channel from a sensor of the selected interfering impurity, for example, the moisture sensor.

— finishing the optical scheme of the sensor to apply more selective, correlative methods of measurement [22,23];

— rejecting the reference channel $3.9\,\mu$m and measuring the current zero level by means of an additional gas channel. In this case, the additional gas channel provides periodic supply of clean filtered air and an analysis algorithm is based on comparison of the signals of the main and additional gas channels. The reference channel $3.9\,\mu$m can also be rejected when using the measurement and reference spectrum channels having similar characteristics of the IR filters, but a different length of the optical path [13].

The said solutions increase the sensor price, but it is unavoidable for improved quality thereof.

Conclusion

The designed optical scheme of the small-sized sensor of carbon monoxide, with the threshold sensitivity of $1\,\text{mg/m}^3$. The overall dimensions of the scheme were $75 \times 35 \times 30\,\text{mm}$, with the optical path length of 10 cm. The said measurement error is theoretically ensured by: using the fast light-emitting diodes and the low-noise photodiodes, the high transmission capacity of the optical scheme with low vignetting losses and effective noise filtration outside the operating frequency of the light-emitting diode. The use of the additional reference channel in the sensor made it possible to introduce self-calibration of the sensor, thereby creating the long-term stability of the measurements. Thermal stabilization of the light-emitting diode and the photodiode of the sensor was applied to determine, by the calculation, the stability of the measurement error within the operating temperature range of $0-50^\circ$C.The parameters of the narrow-band IR filters, which provide acceptable sensitivity to CO, have been optimized. As a result of the calculation, it has been confirmed that the transmittance spectrum of real filters was necessary. It made it possible to take into account the influence of the interfering impurities around the „tails“ of the IR filter. The calculation has ended in determining the limits of applicability of the designed sensor and proposing ways of improvement of the measurement selectivity.

References

[1] S.I. Indiaminov, A.A. Kim. Sudebnaya meditsina, **6** (4), 4 (2020) (in Russian). DOI: 10.19048/fm344 [S.I. Indiaminov, A.A. Kim. Russian J. Forensic Medicine, **6** (4), 4 (2020). DOI: 10.19048/fm344].
[2] GOST R 57717-2017 [Electronic source]. URL: https://docs.cntd.ru/document/1200147096
[3] GOST R 1.2.3685-21 [Electronic source]. URL: https://docs.cntd.ru/document/573500115?marker=6540IN.
[4] J. Mikolajczyk, Z. Bielecki, T. Stacewicz, J. Smulko, J. Wojtas, D. Szabra, L. Lentka, A. Prokopiuk, P. Magryta. Metrol. Meas. Syst., **23** (5), 205 (2016). DOI: 10.1515/mms-2016-0026
[5] J. Mikołajczyk, J. Wojtas, Z. Bielecki, T. Stacewicz, D. Szabra, P. Magryta, A. Prokopiuk, A. Tkacz, M. Panek. Metrol. Meas. Syst., **23** (3), 481 (2016). DOI: 10.1515/mms-2016-0030
[6] J. Wong, M. Schell. Sensor Review, **31** (1), 70 (2011). DOI: 10.1108/02602281111099116
[7] Datasheet smartGAS [Electronic source]. URL: https://www.smartgas.eu/en/
[8] Datasheet Cubic [Electronic source]. URL: https://en.gassensor.com.cn/
[9] Datasheet Promisense [Electronic source]. URL: http://en.promisense.com/index.php
[10] Datasheet Euro-Gas [Electronic source]. URL: https://eurogas.ie/products/gas-detection/gas-sense/analogue-gas-detectors/
[11] Datasheet Ecotech [Electronic source]. URL: https://www.acoem.com/australasia/products/ambient-air/air-quality-gas-analyzers/co-analyser/serinus-30/

[12] Datasheet Horiba [Electronic source]. URL: https://www.horiba.com/int/process-and-environmental/products/detail/action/show/Product/pg-300-series-257/
[13] J. Hodgkinson, R. Tatam. Meas. Sci. Technol., **24** (1), 012004 (2012). DOI: 10.1088/0957-0233/24/1/012004
[14] C. Hummelgerd, I. Bryntse, M. Bryzgalov, J. Henning, H. Martin, M. Noren, H. Rudjegerd. Urban Climate, **14** (3), 342 (2015). DOI: 10.1016/j.uclim.2014.09.001
[15] K. Li, B. Wang, M. Yuan, Z. Yang, C. Yu, W. Zheng. Int. J. Environ. Res. Public Health., **19** (19), 12828 (2022). DOI: 10.3390/ijerph191912828
[16] Ioffe LED [Electronic source]. URL: http://www.ioffeled.com
[17] S. Fanchenko, A. Baranov, A. Savkin, V. Sleptsov. In: IOP Conf. Ser.: Mater. Sci. Eng. (IOP Publishing, 2016), vol. 108. DOI: 10.1088/1757-899X/108/1/012036.
[18] Zemax EE 2006 version, optical raytrace software package, Zemax, Redmond, WA, USA, 2006.
[19] Hitran [Electronic source]. URL: https://hitran.iao.ru/
[20] G.G. Ishanin, E.D. Pankov, V.P. Chelibanov. Priemniki izlucheniya, (Papirus, SPb., 2003) (in Russian).
[21] NIST Chemistry WebBook [Electronic source]. URL: https://webbook.nist.gov/chemistry
[22] P. Chambers, E. Austin, J. Dakin. Meas. Sci. Technol., **15** (8), 1629 (2004). DOI: 10.1088/0957-0233/15/8/034
[23] E. Vargas-Rodrygueza, H. Rutt. Sensors and Actuators B, **137**, 410 (2009). DOI: 10.1016/j.snb.2009.01.013

Translated by M.Shevelev